IHTC14-22695

HEAT AND MASS TRANSFER IN A PERMEABLE FABRIC SYSTEM UNDER HOT AIR JET IMPINGEMENT

Sangsoo Lee
Department of Mechanical Engineering
University of Nevada, Reno
Reno, NV, USA

Chanwoo Park
Department of Mechanical Engineering
University of Nevada, Reno
Reno, NV, USA

Devdatta Kulkarni
Advanced Cooling Technologies, Inc.
Lancaster, PA, USA

Sanjida Tamanna
Advanced Cooling Technologies, Inc.
Lancaster, PA, USA

Ted Knox
Air Force Research Laboratory
Wright-Patterson AFB, OH, USA

ABSTRACT

Heat and mass transfer in a permeable fabric system used for Personal Protective Equipment (PPE) was investigated using hot air jet impingement conditions to mimic the jet exhaust of Short Take-Off and Vertical Landing (STOVL) aircraft. The STOVL aircraft uses a thrust-vectoring nozzle of the jet engine and a lift fan in order to vertically land and take off a short runaway. The jet engine exhaust is a new kind of thermal hazard for military personnel operating within an affected zone of the jet exhaust.

An experimental approach was used to measure the thermal response of a fabric system consisting of permeable fabric samples and air pocket using a high-speed jet impingement. The jet impingement conditions consisted of two different temperatures: one of 100°C and another of 200°C at a jet impingement velocity of 32 m/s. Air was used as the working fluid. In this study, two permeable fabrics, (NOMEX IIIA and Cotton) commonly used for the Personal Protective Equipment (PPE) were investigated. The physical properties (porosity, permeability, Ergun coefficient, and density) and the thermo-physical properties (thermal diffusivity, thermal conductivity, and specific heat) of the fabrics were measured.

A one-dimensional, two-medium formulation assuming thermal non-equilibrium between solid (fabric) and gas (air) phases in the fabric layer was used for the numerical analysis. The measurement results from the fabric experiment were used to define boundary conditions and adjust various heat transfer correlations and input data used in the numerical model.

The experimental and numerical results of the temperatures of the fabric system were compared. The effects of the air temperature of the jet impingement on the thermal response of the fabric system were discussed.

1. INTRODUCTION

The Short Take-Off and Vertical Landing (STOVL) aircraft impinges a hot, high-speed jet exhaust directly to ground which could cause severe thermal injuries to the military crews operating within an affected zone of the jet exhaust. Proper Personal Protective Equipment (PPE) is essential for providing a thermal protection (i.e., insulation) to the military personnel to prevent from skin burn injuries. The thermal insulation performance of the PPE fabrics is essential for proper thermal protection.

The previous work done by other researchers on personal thermal protection was mostly focused on radiative heating due to fire. Knox et al. [1,2,3] have documented comprehensive results from computer simulation and experimental research for human skin burn. The skin burn simulation code (named BURNSIM) for an one-dimensional, bio-heat transfer calculation across the multiple layers of human skin was developed to evaluate various thermal hazard conditions such as rocket plumes from ejection seats of jet fighter pilots, shoulder launched weapons, nuclear flash and live fire [4]. Mell and Lawson [5] analyzed an one-dimensional heat transfer case for the non-permeable fabric of firefighter's protective clothing under radiant heat fluxes. Barker et al. [6] reported that from a fabric experiment using radiant heating, gas permeation through PPE fabrics dramatically increases the convective heat transfer in the fabric yarn and causes a direct heating of human skin that was in contact with the fabrics. They also reported that moisture in the fabrics significantly increases skin burn injury due to the hot water vapor.

Hirschler [7] experimentally measured the thermal insulation performance of two PPE fabrics in dry and damp conditions under a direct contact with heated bricks over 400°C.

The results showed that the temperatures of the dry fabrics quickly increase during the initial period of time and then slowly approaches a steady-state temperature. The rates of the temperature increased at the back side of the fabric were varied by the thermal conductivity of the fabrics used for the experiment. The temperature response of the damp fabrics showed a noticeable plateau at the water boiling temperature and a slow increase to the steady-state condition.

Song [8] measured an air gap distribution on a manikin body with a three-dimensional body scanning technique to evaluate a thermal protection performance of PPE fabrics subject to a flash fire. The best result to protect human body with one-layer protective garment was obtained when the air gap was 7~8 mm. Kim et al. [9] measured the distribution of the air gap around a surface of a manikin body to investigate the effect of the air gap in protective clothing under radiative heating. The best thermal protective performance under a flame radiation of 84 kW/m^2 for 6 seconds was obtained with an air gap of 6.4 mm. Liter et al. [10~12] presented experimental and numerical results of the heat transfer in air bag fabrics using the conditions of air bag deployment. The numerical model considering internal and surface convective heat transfer due to jet impingement flows was used to predict thermal responses of the airbag fabrics during air bag deployment. There are a handful of industrial standards describing specific procedures and conditions to test thermal responses of PPE fabrics and clothing materials under various heating conditions [13-15].

For this study, an experimental apparatus was built to measure the temperature response of two permeable fabrics using high-speed, high-temperature air jet impingement as the heating source. The measurement results from the fabric experiment were used to determine boundary conditions and validate the numerical results of the heat transfer calculation based on one-dimensional, two-medium treatment assuming thermal non-equilibrium between solid (fabric) and gas (air) phases.

NOMENCLATURE

A	area [m^2]
B	average planar yarn width [m]
C	coefficient
c	specific heat [J/g-K]
D	diameter or hydraulic diameter [m]
H	height [m]
h	heat transfer coefficient [W/m^2-K]
K	permeability [m^2]
k	thermal conductivity [W/m-K]
L	length [m]
$\dot{m}$	mass flow rate [kg/s]
N	weave count [number of yarns per inch]
P	pressure [Pa]
Pr	Prandtl number
$\dot{Q}$	heat transfer rate [W]
R	gas constant [J/kg-K]
Re	Reynolds number

T	temperature [°C or K]
t	time [s]
u	velocity [m/s]
V	volume [m^3] or velocity [m/s]
W	width [m]
x	x-directional dimension [m]

Superscripts and Subscripts

1,2,..	indices
ap	air pocket
amb	ambient
avg	averaged
c	cross-sectional
cp	cold plate
D	Darcian
E	Ergun
fab	fabric
front	front surface of the fabric
g	gas
h	horizontal
i	initial
in	inlet
jet	impinging jet
leak	leakage
meas	measured
nz	nozzle
out	outlet
p	pressure
r	ratio
rear	rear surface of the fabric
s	solid
sg	solid-gas interface
ss	steady-state
v	vertical

Greeks and Symbols

α	thermal diffusivity [cm^2/s]
ε	porosity
μ	viscosity [kg/m-s]
ρ	density [kg/m^3]
τ	time constant [s]

2. FABRIC PROPERTY MEASUREMENT

Two kinds of fabrics (NOMEX IIIA and Cotton/Spandex) were used for this study. The NOMEX fabric has been widely used for various personal protective equipment and clothing for thermal protection because of its flame retardant property. The Cotton/Spandex was chosen as an ordinary fabric used for daily usage. Both fabrics were permeable to a gas flow. The physical properties (porosity, permeability, and Ergun coefficient) and the thermo-physical properties (thermal conductivity, density, and specific heat) of the fabrics were measured.

2.1. Measurement of Thermophysical Properties of Fabrics

The thermal diffusivities (α) of the fabrics were measured by the laser flash method [16] in a vacuum jar, which uses a short laser burst as the heating source. The specific heat capacity (c_p) of the fabrics was measured using a Differential Scanning Calorimeter (DSC) [17]. The property measurement was performed up to 200°C which is the maximum temperature of the air impingement flow used in this study. The density of the fabrics (ρ) was determined from the measured volume and mass of the fabric samples. The thermal conductivities (k) of the fabrics were calculated from the product of three measured quantities, i.e., $k = \alpha \rho c_p$. Since the fabric samples were tested in a vacuum jar for the thermal diffusivity measurement, the calculated thermal conductivity is assumed to be the thermal conductivity only for the solid phase of the fabrics.

Figure 1 shows the thermophysical property variations of the fabrics with temperature. Table 1 lists the measured thermophysical properties for the NOMEX and Cotton/Spandex fabrics.
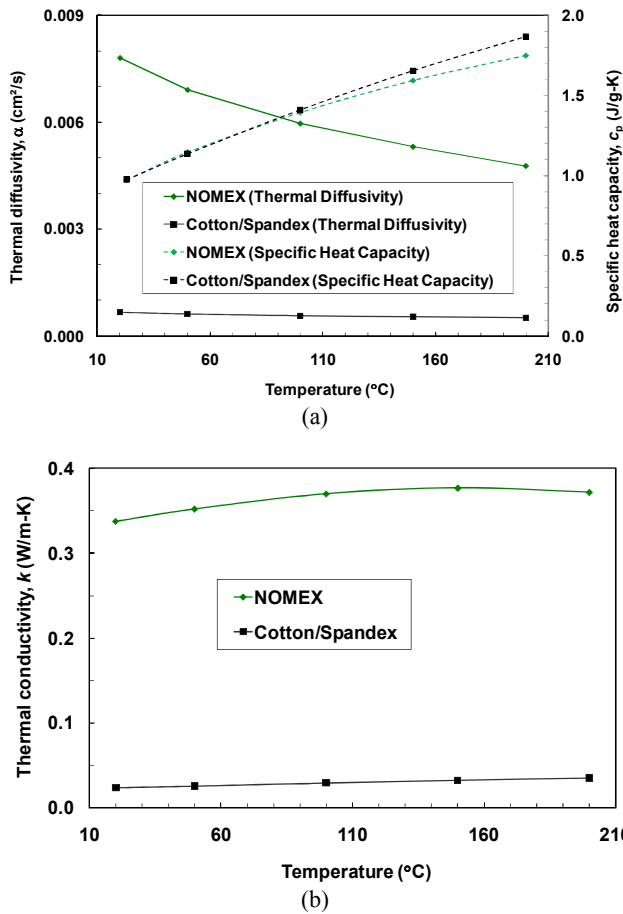

(a)

(b)

Figure 1 Thermophysical property variations of NOMEX and Cotton/Spandex fabrics with temperature. (a) measured thermal diffusivity and specific heat and (b) calculated thermal conductivity

Table 1 Thermophysical properties for two fabrics considered for this work

	Units	NOMEX IIIA				
		23°C	50°C	100°C	150°C	200°C
ρ	kg/m³	446.0	-	-	-	-
α	cm²/s	0.00780†	0.00690	0.00596	0.00531	0.00477
c_p	J/g-K	0.970	1.144	1.392	1.592	1.748
k‡	W/m-K	0.337	0.352	0.370	0.377	0.372
		Cotton/Spandex				
		23°C	50°C	100°C	150°C	200°C
ρ	kg/m³	365.0	-	-	-	-
α	cm²/s	0.000667†	0.000620	0.000572	0.000543	0.000520
c_p	J/g-K	0.976	1.136	1.410	1.654	1.868
k‡	W/m-K	0.0238	0.0257	0.0294	0.0328	0.0354

† The thermal diffusivity was measured at 20°C.

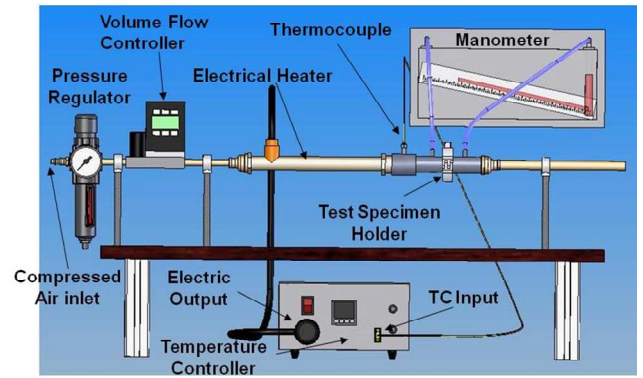‡ The thermal conductivity was calculated by $k = \alpha \rho c_p$.

Figure 2 Schematics of the fabric permeability measurement apparatus

2.2. Measurement of Permeability of Fabrics

The permeability of the fabrics directly affects the gas (e.g. air or moisture) permeation through the fabric layer and thus the heat transfer in a fabric system. Figure 2 shows the schematic of the experimental apparatus for the fabric permeability measurement using air as the working fluid. The permeability measurement was conducted at various temperatures, because fabric shrinkage and thermophysical properties of air are changed by temperature.

Using the modified Forchheimer equation, the pressure drop in a fabric layer is given by

$$-\frac{dP}{dx} = \frac{\mu}{K} u_D + \frac{\rho C_E}{\sqrt{K}} u_D^2 \qquad (2)$$

where, P is the air pressure [Pa], u_D is the Darcian velocity [m/s], ρ is the air density [kg/m³], μ is the air viscosity [kg/m-s], K is the permeability [m²] and C_E is the Ergun coefficient.

The density of air is calculated from ideal gas law by

$$\rho = \frac{P}{RT} \qquad (3)$$

where, R is the gas constant for air, which is 287 J/kg-K and T is the temperature of air in Kelvin.

After integrating the pressure drop equation Eq. (2) along with the ideal gas law over the fabric layer thickness, the modified Forchheimer equation becomes

$$\frac{A_c(P_{in}^2 - P_{out}^2)}{2L\dot{m}\mu RT} = \frac{1}{K} + \frac{C_E}{\sqrt{K}}\frac{\rho u_D}{\mu} \qquad (4)$$

where, P_{in} is the upstream pressure, P_{out} is the downstream pressure of the fabric layer, L is the fabric thickness and A_c is the cross-sectional area of the fabric for air flow. By plotting Eq. (4) in a *x-y* graph format, the permeability (K) and Ergun coefficient (C_E) are determined from the intercept ($1/K$) and the slope ($C_E/\sqrt{K}$) of the line of the graph. Table 2 lists the values of the measured permeability and Ergun coefficient for the NOMEX and Cotton/Spandex fabrics.

3. EXPERIMENTAL SETUP AND PROCEDURE

The experimental setup used for the thermal response measurement of permeable fabrics using hot air jet impingement conditions is shown in Figure 3. An in-house compressed air (80 psi) regulated by a pressure regulator was used to achieve an air velocity of 32 m/s impinging in front of the fabric. Two in-line electrical heaters (total heater power of 3 kW) were used to heat the air flow up to temperatures of 100°C or 200°C in front of the fabric.

The diameter of the air nozzle was 20.6 mm and the distance between the nozzle tip and the front fabric surface was 76.2 mm. A pitot tube was used to measure the air velocity and pressure of the impinging flow in front of the fabric as shown in Figure 3. There exists a time delay (~2.5 seconds) for the air jet impinging flow to reach the target temperature in front of the fabric due to the jet flow development.

The fabric sample (150 mm × 150 mm) was clamped to the fabric holder using a thin square frame. The fabric sample was covered using a high-temperature tape outside a circular area with a diameter of 28.5 mm at the center of the fabric for air flow. The partial covering on the fabric sample was necessary to prevent a reverse flow out of the air pocket

Table 2 Values of the permeability and Ergun coefficients for the NOMEX and Cotton/Spandex fabrics

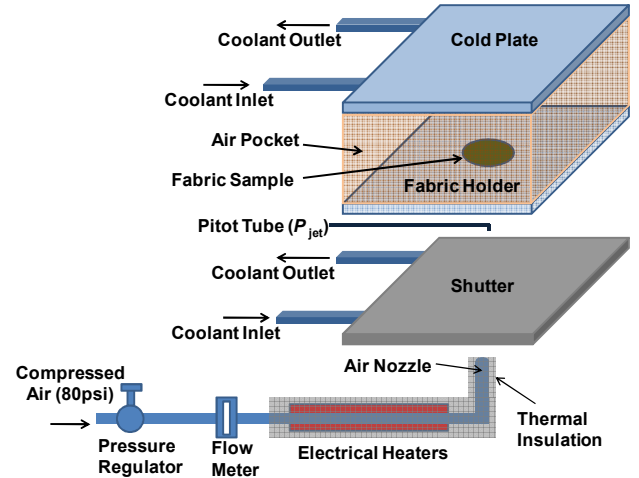|	Units	NOMEX IIIA	Cotton/Spandex
T	°C	15.0	15.0
ε	-	0.626	0.75
K	m²	0.454×10^{-10}	1.56×10^{-10}
C_E	-	2.11	1.17

Figure 3 Schematic of the experimental setup for fabric thermal response measurement

due to the jet impingement over the large fabric sample surface. The air pocket between the fabric sample and the rear wall of the enclosure has about 6mm thickness. The air pocket is similar to the air gap between protective clothing and human skin. The air pocket was not perfectly sealed to allow a small leakage to the ambient through the narrow gaps in the air pocket walls, to simulate what actually happens in the protective garment.

The rear wall of the air pocket consists of a cold plate (110 mm × 110 mm) which was maintained at a constant temperature of 15°C by a cooling loop. The cold plate was used to remove the heat carried by the air permeating through the fabric into the air pocket. The cold plate mimics a human skin at a body temperature. The side walls of the air pocket were built using a high-temperature ceramic insulation material to prevent heat loss to ambient.

The fabric holder assembly as shown in Figure 4(a) was fabricated to hold and position a fabric sample rigidly against the hot air impinging flow according to the industrial standards of ISO 17492 [13] and ASTM D 4108-8 [14]. In order to consistently stretch the fabric sample each testing, a tension meter was used to measure the deflection of the fabric samples during fabric installation.

Figure 4(b) shows the water-cooled shutter actuated by a pneumatic plunger for consistent opening and closing. The shutter (203 mm × 203 mm) placed between the air nozzle and the fabric sample was to prevent a premature heating of the fabric by the hot air impingement prior to testing. The shutter is also shown in Figure 3. The opening and closing times of the shutter were measured to be 92 ms and 80 ms respectively.

The locations of thermocouples (K-type) used in the fabric system are shown in Figure 5. A thermocouple (T_{jet}) was installed to measure the impinging air temperature before
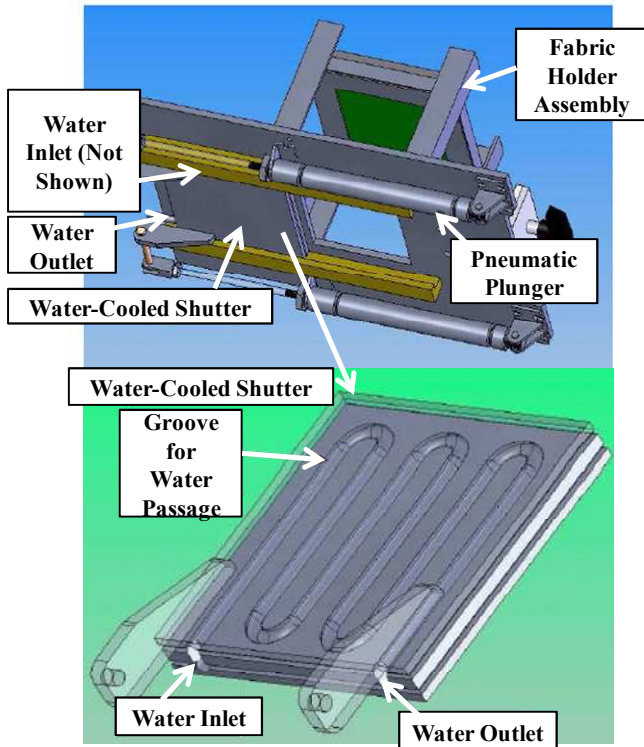
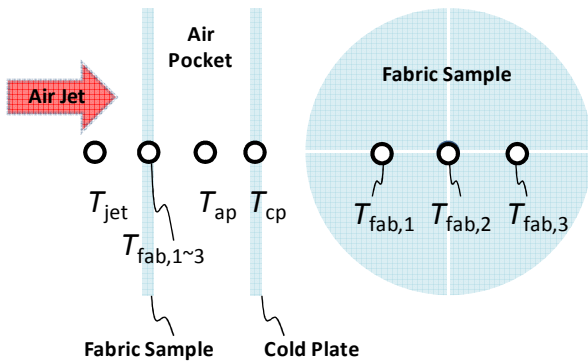Figure 4 (a) Fabric holder assembly and (b) water-cooled, pneumatically actuated shutter

Figure 5 Schematic views of locations of the thermocouples used for the experiment

hitting the fabric. Three thermocouples ($T_{fab,1} \sim T_{fab,3}$) were installed on the front and back surfaces of the fabric sample.

The thermocouple wires of the diameter of 0.127 mm were butt-welded to form a tiny bead and then woven into the fabric layer and the thermocouple bead was pressed down against the fabric surface for a better thermal contact. Then the thermocouple wires were pulled tightly and attached to the edge of the fabric sample using a high temperature tape. The air pocket temperature (T_{ap}) and the cold plate temperature (T_{cp}) were also measured. The data was stored in a computer using a high-speed data acquisition system every 2 ms.
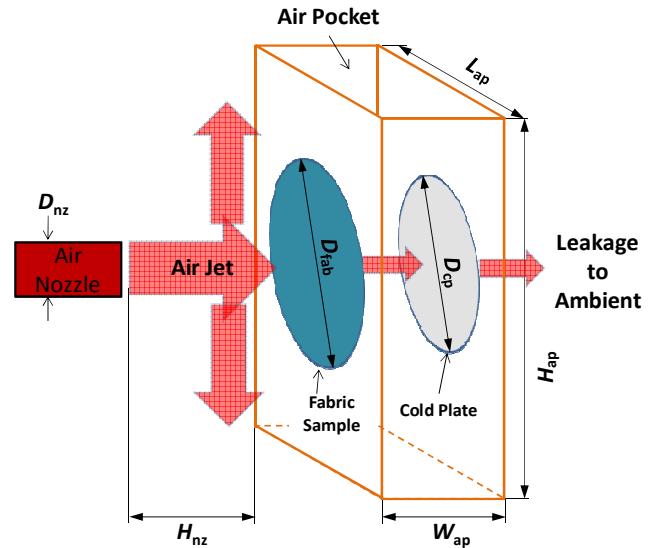

Figure 6 Schematic diagram of the fabric experimental setup

The experiment started by first applying a hot air jet impingement onto the water-cooled shutter which was initially closed for 5 seconds to prevent premature heating of the fabric prior to testing. When the shutter was quickly opened by a pneumatic plunger, the air impingement flow reached the front fabric surface and the pre-set temperature of the air jet impinging flow was achieved within about 2.5 seconds. The fabric sample was exposed to the air jet impingement for 30 seconds until the shutter was automatically closed. Subsequent test was performed after the shutter temperature is recovered to the initial temperature.

4. NUMERICAL MODELING AND FORMULATION

A numerical model based on one-dimensional, two-medium treatment assuming thermal non-equilibrium between fabric and air phases was used to predict the thermal responses of the fabric system. The measurement results from the fabric thermal response experiment were used to determine boundary conditions and calibrate heat transfer correlations used in the numerical model.

Figure 6 shows the schematic diagram of the fabric system used for the numerical modeling. The air jet impingement (T_{jet}) from a nozzle is applied to the front surface of the fabric. The air flows through the permeable fabric into an air pocket and was treated as a one-dimensional flow. Table 3 lists the dimensional specifications of the fabric experimental setup and the fabrics used in the study.

The computational domain and grid system of the numerical model is shown in Figure 7. The heat transfer coefficients at various locations of the system are also shown. Each node (denoted as a dot) represents a temperature node. The fabric layer has two surface nodes and three volume nodes across the fabric thickness. The air pocket (T_{ap}) behind the fabric was also modeled as a gas volume of a uniform temperature by assuming

Table 3 Dimensional specifications of the fabric experimental setup and fabrics

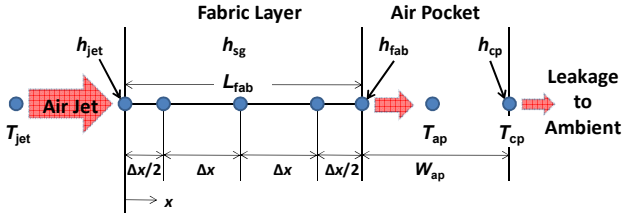| Fabric Experimental Setup			
	Unit		
D_{nz}	mm	20.6	
H_{nz}	mm	76.2	
L_{ap}	mm	101.5	
H_{ap}	mm	101.5	
W_{ap}	mm	6.0	
Fabric			
	Unit	NOMEX III$_A$	Cotton/Spandex
D_{fab}	mm	22.5	22.5
D_{cp}	mm	22.2	22.2
L_{fab}	mm	0.340	0.797
N_h	-	60	40
N_v	-	60	60
B	mm	0.320	0.320
D_y	mm	0.222	0.355
A_{sg}/V_{fab}	m^{-1}	15,798	8,978

Figure 7 Computational domain of the one-dimensional model and its grid system showing temperature nodes and heat transfer coefficients

a perfect mixing. The air volume in the air pocket is cooled by a water-cooled, cold plate (T_{cp}) which was maintained at 15°C.

Empirical correlations were used to calculate the heat transfer due to the jet impingement and internal flow through the fabric layer. The radiation heat transfer was neglected because the convective heat transfer was the dominant heat transfer mode for the temperature range considered for this study.

The governing equations and initial and boundary conditions used for the one-dimensional model are discussed below.

(1) Governing Equations for Gas Phase in the Fabric Layer

The mass, momentum and energy conservation equations are given by

$$\varepsilon \frac{\partial \rho_g}{\partial t} + \frac{\partial}{\partial x}(\rho_g u_D) = 0 \tag{5}$$

$$\frac{\partial(\rho_g u_D)}{\partial t} + \frac{1}{\varepsilon}\frac{\partial(\rho_g u_D^2)}{\partial x}$$
$$= \frac{\partial}{\partial x}\left(\mu \frac{\partial u_D}{\partial x}\right) - \varepsilon \frac{dP}{dx} - \varepsilon \frac{\mu}{K}u_D - \varepsilon\rho_g \frac{C_E}{K^{1/2}}u_D^2 \tag{6}$$

$$\varepsilon(\rho c_p)_g \frac{\partial T_g}{\partial t} + (\rho c_p)_g u_D \frac{\partial T_g}{\partial x}$$
$$= \frac{\partial}{\partial x}\left(\varepsilon k_g \frac{\partial T_g}{\partial x}\right) - h_{sg}\left(\frac{A_{sg}}{V_{fab}}\right)(T_g - T_s) \tag{7}$$

where, T_g and T_s are the volume-averaged temperatures for gas phase (air) and solid phase (fabric) in the fabric layer. u_D is the Darcian velocity. ε is the porosity of the fabric layer. K is the permeability and C_E is the Ergun coefficient used for the momentum equation in the fabric layer. The temperature-dependent properties of air and fabric were used for the calculation. h_{sg} is the interstitial convective heat transfer coefficient for the fabric and gas phases. A_{sg} is the surface area of the fabric layer and was calculated by

$$A_{sg} = 0.0254(N_h + N_v)\pi D_y \tag{8}$$

$$D_y = \frac{2L_{fab}B}{L_{fab} + 2B} \tag{9}$$

where D_y is the hydraulic diameter of a yarn of the fabric weave and is approximated as the hydraulic diameter of a rectangular tube with a height of one half the fabric thickness L, and width B of the average width of the yarn along the plane of the fabric surface [10].

(2) Governing Equation for Fabric Phase in the Fabric Layer
The energy conservation equation for the fabric phase is given by

$$(1-\varepsilon)(\rho c_p)_s \frac{\partial T_s}{\partial t} = \frac{\partial}{\partial x}\left((1-\varepsilon)k_s \frac{\partial T_s}{\partial x}\right) + h_{sg}\left(\frac{A_{sg}}{V_{fab}}\right)(T_g - T_s) \tag{10}$$

(3) Ideal Gas Law
Air was modeled as an ideal gas law.

$$\rho_g = \frac{P}{R T_g} \tag{11}$$

(4) Initial Conditions

$$u_D = 0, \; T_g = T_s = T_i \quad \text{at} \; t = 0 \tag{12}$$

(5) Boundary Conditions
(i) Front Surface of the Fabric ($x = 0$)
The pressure in front of the fabric was measured using a Pitot tube and a manometer to determine the pressure boundary condition. The measured pressure was curve-fitted using a dynamic pressure formulation and is given by

$$p_{jet} = C_{jet,p}\rho_{jet}\left(\frac{1}{2}V_{jet}^2\right) \tag{13}$$

where $C_{jet,p}$ is the correction coefficient for the pressure equation. V_{jet} is the velocity of the jet impingement flow

measured by the Pitot tube. The velocity of the jet impingement used for this study was 32 m/s.

The measured temperature of the jet impingement flow in front of the fabric was also curve-fitted by

$$T_{\text{jet}} = T_{\text{i}} + (T_{\text{jet,ss}} - T_{\text{i}})(1 - e^{-t/\tau}) \tag{14}$$

where T_{i} is the initial temperature of the jet impingement flow. $T_{\text{jet,ss}}$ is the steady-state temperature of the jet impingement flow. τ is the time-constant required for the jet flow development and was determined by curve-fitting the measured air temperature (T_{jet} as shown in Figure 5) impinging on the front surface of the fabric. From the curve-fitting, $\tau = 0.526$ seconds. The thermal boundary conditions for air flow and fabric surface in front of the fabric are given by

$$T_{\text{g}} = T_{\text{jet}} \tag{15}$$

$$-k_{\text{s}} \frac{dT_{\text{s}}}{dx}\bigg|_{x=0} = h_{\text{jet}}(T_{\text{jet}} - T_{\text{s}}|_{x=0}) \tag{16}$$

here, h_{jet} is the heat transfer coefficient at the front surface of the fabric due to the jet impingement flow. The empirical correlation for h_{jet} is discussed in the following section.

(ii) Rear Surface of the Fabric ($x = L_{\text{fab}}$)

The rear surface of the fabric is exposed to the air pocket. The heat transfer boundary conditions at the rear surface of the fabric ($x = L_{\text{fab}}$) are given by

$$\frac{dT_{\text{g}}}{dx}\bigg|_{x=L_{\text{fab}}} = 0 \tag{17}$$

$$-k_{\text{s}} \frac{dT_{\text{s}}}{dx}\bigg|_{x=L_{\text{fab}}} = h_{\text{fab}}(T_{\text{s}}|_{x=L_{\text{fab}}} - T_{\text{ap}}) \tag{18}$$

here, h_{fab} is the convective heat transfer coefficient at the rear surface of the fabric due to the air flow in the air pocket. The equation for h_{fab} is discussed in the following section.

(6) Governing Equations for the Air Pocket
The mass conservation equation is given by

$$V_{\text{ap}} \frac{d\rho_{\text{g}}}{dt} = \dot{m}_{\text{g,in}} - \dot{m}_{\text{g,out}} \tag{19}$$

where,

$$\dot{m}_{\text{g,in}} = \rho_{\text{g}} A_{\text{fab}} u_{\text{D}}\big|_{x=L_{\text{fab}}} \tag{20}$$

$$\dot{m}_{\text{g,out}} = C_{\text{leak}} \frac{\rho_{\text{g}}}{\mu_{\text{g}}} (P_{\text{ap}} - P_{\text{amb}}) \tag{21}$$

here, the air leakage rate ($\dot{m}_{\text{g,out}}$) is determined by the pressure difference between the air pocket and ambient. C_{leak} is 1.62725×10^{-12} [m³] for the NOMEX fabric.

The energy conservation equation for the air pocket is given by

$$(\rho V c_{\text{p}})_{\text{ap}} \frac{dT_{\text{ap}}}{dt} = \dot{Q}_{\text{g,in}} - \dot{Q}_{\text{g,out}} + \dot{Q}_{\text{fab,rear}} - \dot{Q}_{\text{cp}} \tag{22}$$

where,

$$\dot{Q}_{\text{g,in}} = (\dot{m} c_{\text{p}} T)_{\text{g,in}} \tag{23}$$

$$\dot{Q}_{\text{g,out}} = (\dot{m} c_{\text{p}} T)_{\text{g,out}} \tag{24}$$

$$\dot{Q}_{\text{fab,rear}} = h_{\text{fab}} A_{\text{fab}} (1-\varepsilon)(T_{\text{s}}|_{x=L_{\text{fab}}} - T_{\text{ap}}) \tag{25}$$

$$\dot{Q}_{\text{cp}} = h_{\text{cp}} A_{\text{cp}} (T_{\text{ap}} - T_{\text{cp}}) \tag{26}$$

here, $\dot{Q}_{\text{g,in}}$ is the enthalpy influx into the air pocket and $\dot{Q}_{\text{g,out}}$ is the enthalpy outflow from the air pocket to ambient by the air leakage. $\dot{Q}_{\text{fab,rear}}$ is the convective heat transfer at the rear surface of the fabric. $\dot{Q}_{\text{cp}}$ is the convective heat transfer at the cold plate which was maintained at a constant temperature of 15°C.

The heat transfer coefficients (h_{jet}) of the jet impingement flow at the front side of the fabric was calculated using a empirical correlation for a jet impingement on a "solid" surface with a single round nozzle developed by Martin [18]. It was assumed that the heat transfer of the jet impingement on "permeable" fabric surfaces can be estimated by one for a solid surface because the air flow rate permeating through the fabric surface is negligible as compared to the flow rate of the jet impingement from the nozzle. The heat transfer coefficient is determined by

$$h_{\text{jet}} = C_{\text{jet}} \frac{k_{\text{jet}}}{D_{\text{jet}}} GF \text{Pr}_{\text{jet}}^{0.42} \quad \begin{cases} 2\times10^3 \le \text{Re}_{\text{D,nz}} \le 4\times10^5 \\ 2 \le \left(H/D\right)_{\text{nz}} \le 12 \\ 0.004 \le A_{\text{r}} \le 0.04 \end{cases} \tag{27}$$

$$G = 2A_{\text{r}}^{\frac{1}{2}} \frac{1 - 2.2A_{\text{r}}^{\frac{1}{2}}}{1 + 0.2\left[\left(H/D\right)_{\text{nz}} - 6\right]A_{\text{r}}^{\frac{1}{2}}} \tag{28}$$

$$F = 2\text{Re}_{\text{D,nz}}^{\frac{1}{2}} \left(1 + 0.005\text{Re}_{\text{D,nz}}^{0.55}\right)^{\frac{1}{2}} \tag{29}$$

$$\text{Re}_{\text{D,nz}} = \frac{\rho_g D_{nz}}{\mu_g} \tag{30}$$

Here, H_{nz} is the distance between the air nozzle tip to the front surface of the fabric. D_{nz} is the nozzle diameter. A_{r} is the ratio of the nozzle area to the surface area of the fabric. A correction factor (C_{jet}) is used for a better agreement between the prediction and the measurement results.

The heat transfer at the cold plate in the air pocket can be also calculated by the jet impingement correlation because of the similar condition. For the calculation of the heat transfer coefficient (h_{cp}) of the cold plate, the thickness of the air pocket (W_{ap}) which is the distance between the rear surface of the fabric and the cold plate is used as the nozzle distance (H_{nz}). The diameter of the fabric opening area (D_{fab}) is the nozzle

diameter. C_{cp} is the correction factor for the heat transfer coefficient (h_{cp}) at the cold plate.

For the heat transfer calculation by the gas flow in the permeable fabric, the semi-empirical correlation developed by Whitaker [19] for a packed bed of small particles was used and is given by

$$h_{sg} = C_{sg} \frac{k_g}{D_y} \frac{1-\varepsilon}{\varepsilon} \left(0.4 \operatorname{Re}_{D,y}^{\frac{1}{2}} + 0.2 \operatorname{Re}_{D,y}^{\frac{2}{3}} \right) \operatorname{Pr}^{0.4} \qquad (31)$$

$$\operatorname{Re}_{D,y} = \frac{\rho_g u_D D_y}{\mu_g (1-\varepsilon)} \qquad (32)$$

here, D_y is the hydraulic diameter of the fabric and determined by Eq. (9). C_{sg} is the correction factor for the interstitial convective heat transfer coefficient. The heat transfer coefficient (h_{fab}) at the rear surface of the fabric was also calculated using the same correlation. C_{fab} is the correction factor for the convective heat transfer coefficient.

The governing equations of the mass, momentum and energy conservations for the fabric system were solved using a FORTRAN code based on the SIMPLER algorithm. An IMSL subroutine (IVPAG) as an initial value problem solver was used to solve the governing equations of the air pocket. The minimum time step used for the numerical analysis was 0.5 ms. The computation time for a typical case was about 4 hours using a computer with an Intel Core2 Duo processor (2.66 GHz).

5.   RESULTS AND DISCUSSIONS

The conditions used for the study include the air impingement temperatures of 100°C and 200°C and the jet impingement velocity of 32 m/s. Two permeable fabrics (NOMEX and Cotton/Spandex) were tested in this study. The measurement results of the fabric thermal response experiment were used to determine the boundary conditions and calibrate the heat transfer correlations used in the numerical model.

5.1. Model Calibration

For better agreement between numerical and experimental results, a series of calibration for the numerical model was performed by tuning the correction factors for the heat transfer coefficients and boundary conditions. The calibration was conducted against the measurement results based on the baseline case of an impinging air temperature of 200°C for the NOMEX fabric. Table 4 shows the correction factors obtained from the model calibration. The calibrated model was applied for a different impinging air temperature of 100°C without change.

Table 4 Correction factors used for the pressure and temperature boundary conditions, heat transfer correlations

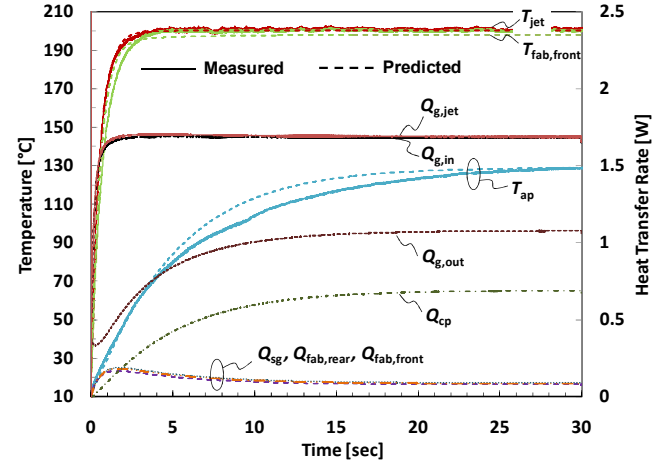| $C_{jet,p}$	C_{jet}	C_{sg}	C_{fab}	C_{cp}
0.375	1.79	1.0	0.2	3.33

Figure 8 Temperature and heat flux variations for the NOMEX fabric under the 200°C air impingement flow

Figure 8 shows the comparison of the temperatures and heat transfer rates from the experimental measurement and numerical prediction for the baseline case of the NOMEX fabric under an air impingement temperature of 200°C. Solid lines are for the measured results and dashed lines are for the predicted results. The temperature of the air impingement flow (T_{jet}) was used as the temperature boundary condition in Eq. (14). The temperatures of (i) front fabric surface ($T_{fab,front}$), and (ii) air pocket (T_{ap}) were compared between the measured (solid line) and predicted (dashed line) results.

As shown in the figure, the fabric temperature ($T_{fab,front}$) rapidly increases and approaches the impinging air temperature of 200°C within about 3 seconds, while the air pocket temperature (T_{ap}) slowly increases to a steady-state temperature of 128°C. The measured and predicted temperatures are in a reasonably good agreement. The air pocket temperature shows the quality of the calibration, because the air pocket temperature is collectively affected by the heat and mass transfers in the air pocket.

The heat fluxes ($\dot{Q}_{g,in}$, $\dot{Q}_{g,out}$, $\dot{Q}_{cp}$, and $\dot{Q}_{fab,rear}$) used in Figure 8 were defined in the previous section of "4. Numerical Modeling and Formulation". $\dot{Q}_{g,jet}$, $\dot{Q}_{fab,front}$ and $\dot{Q}_{sg}$ are defined as

$$\dot{Q}_{g,jet} = (\dot{m} c_p T)_{g,jet} \qquad (33)$$

$$\dot{Q}_{fab,front} = h_{jet} A_{fab} (1-\varepsilon)(T_{jet} - T_{s,x=0}) \qquad (34)$$

$$\dot{Q}_{sg} = h_{sg} A_{sg} (T_g - T_s) \qquad (35)$$

where $\dot{Q}_{g,jet}$ is the enthalpy influx into the fabric by the jet impingement flow. $\dot{Q}_{fab,front}$ is the heat transfer rate at the front surface of the fabric by the jet impingement flow. $\dot{Q}_{sg}$ is
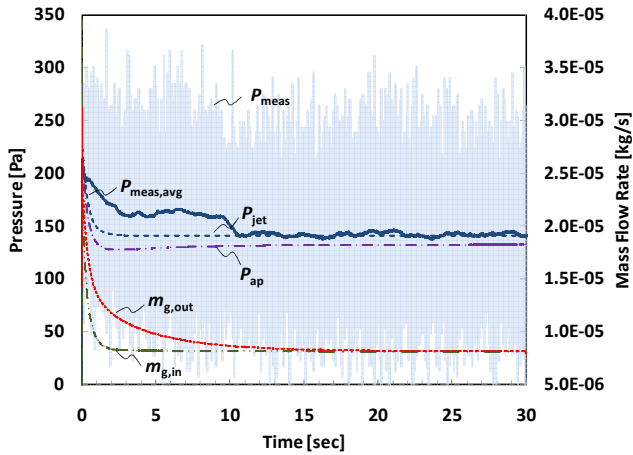
Figure 9 Pressure and mass flow rate variations for the NOMEX fabric under 200°C air impingement flow
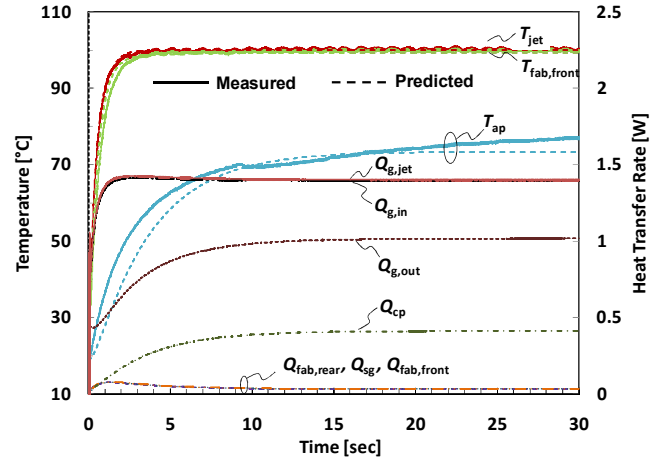

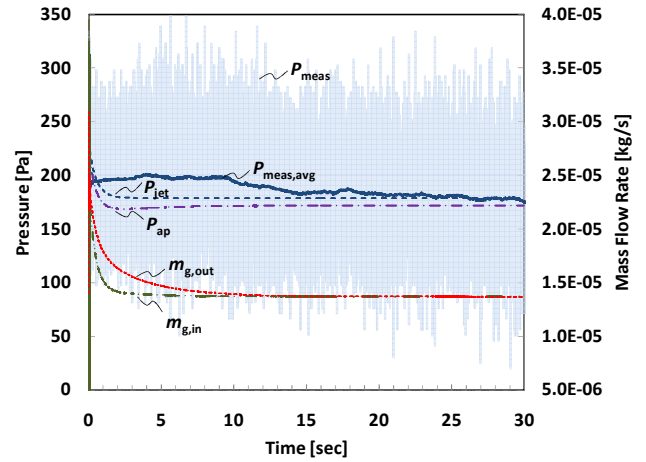Figure 10 Temperatures and heat flux variations for the NOMEX fabric under the 100°C air impingement flow

Figure 11 Pressure and mass flow rate variations for the NOMEX fabric under the 100ºC air impingement flow

the interstitial heat transfer rate between the air flow and the fabric in the fabric layer.

It is observed in Figure 8 that $\dot{Q}_{g,in}$ quickly increases and then converges to the steady state. In contrast, $\dot{Q}_{g,out}$ slowly increases like the temperature of the air pocket. $\dot{Q}_{cp}$ is the heat loss to the cold plate and gradually increases as the air pocket temperature increases. Note that $\dot{Q}_{cp}$ corresponds to the heat transfer rate to human skin and is used as the heat flux boundary for the skin burn calculation. The heat transfer rate ($\dot{Q}_{fab,front}$) at the front surface of the fabric is initially large because of the large temperature difference between the air impingement flow and the fabric surface.

The pressure and mass flow rate variations are shown in Figure 9. P_{meas} is the measured, relative pressure of the impinging air flow in front of the fabric using a Pitot tube. The pressure highly fluctuates because of the turbulent nature of the jet impingement flow on a flexible fabric surface. $P_{meas,avg}$ is the time-averaged pressure of P_{meas} over a time span of 0.1 seconds. It is initially high due to a surge of the jet impingement flow on the fabric surface and then decreases to a steady-state condition. The pressure (P_{jet}) was curve-fitted using Eq. (13) against $P_{meas,avg}$ and was used as the pressure boundary condition in front of the fabric.

The air mass flow rate ($\dot{m}_{g,out}$) defined by Eq. (21) is the mass outflow from the air pocket leaking to ambient. The air leakage rate ($\dot{m}_{g,out}$) is initially higher than the mass influx ($\dot{m}_{g,in}$). This is because the air temperature in the air pocket is lower and thus the air density is higher than those of the air flow into the air pocket. Also note that the pressure difference between the air pocket (P_{ap}) and ambient ($P_{amb} = 0$) is much larger than the pressure difference ($P_{jet} - P_{ap}$) between the air

impinging flow and the air pocket. The mass flow rates eventually are balanced at the steady-state condition.

5.2. Effect of Impinging Jet Temperature

The numerical model calibrated against the baseline case (NOMEX fabric under the impinging air temperature of 200°C) was applied to the case of the air impinging temperature of 100°C. Figure 10 shows the temperature and heat flux variations for the case of the NOMEX fabric under the impinging air temperature of 100°C. Similar trends for the temperature and the heat transfer are observed like the baseline case as shown in Figure 8. The heat transfer ($\dot{Q}_{fab,front}$) at the front side of the fabric and the heat loss ($\dot{Q}_{cp}$) to the cold plate are greatly reduced due to the low temperature of the jet impingement flow. The predicted and measured temperatures of the air pocket (T_{ap}) are in a reasonably good agreement.

Figure 11 shows the pressure and mass flow rate variations for the case of the air jet impingement temperature of 100°C. It is observed that the pressures and mass flow rates were significantly increased because of the larger density of the air flow due to the lower temperature (100°C) as compared with the baseline temperature (200°C). The mass flow rates are balanced at the steady-state condition.

6. CONCLUSIONS

An experimental setup was built to measure the thermal response of the fabric system consisting of a fabric layer and air pocket. The heating source used for the fabric thermal response experiment is the air jet impingement flow with a velocity of 32 m/s at the temperatures of 100°C and 200°C. Two permeable fabrics (NOMEX and Cotton/Spandex) were considered. The fabric physical properties (porosity and permeability) and thermophysical properties (thermal conductivity, density, and specific heat) of the fabrics were measured.

One-dimensional flow and two-medium model was developed and validated against the measurement results of the fabric experiment. The experimental results of the baseline condition using NOMEX fabric under the air jet impingement of 200°C were used to calibrate the numerical model. The predictions from the calibrated model were in good agreement with the experimental results for the cases of the air jet impingement temperature of 100°C.

From the comparison of the measurement and prediction results, it was found that the model can be used to determine various fabric/clothing design parameters (e.g., number of fabric layers and arrangement, fabric thickness and permeability) for an optimum thermal protection and to estimate skin burn coupled with a fabric system under the jet impingement heating condition.

REFERENCES

[1] Knox, F. S., Bonetti, D., and Perry, C. E., 1993, "Users Manual for Burnsim/Burnsim: A Burn Hazard Assessment Model," Technical Report No. 93-13, USAARL.

[2] Knox, F. S., 2007, "An Operational Copy of Burnsim."

[3] Knox, F. S., Reynolds, D. B., Conklin, A., and Perry, C. E., 1998 October "Burn Prediction Using Burnsim and Clothing Models, Model for Aircrew Safety Assessment: Uses, Limitations and Requirements," Proc. RTO Meeting, Dayton, OH, pp. RTO-MP-20.

[4] Knox, F. S., Sauermilch, P. W., Wachfel, T. L., Mcchan, G. R., Trevethan, W. P., Lum, C. B., Brown, R. J., and Alford, L. A., 1979, "A Fire Simulator/Shutter System for Testing Protective Fabrics and Calibrating Thermal Sensors," Technical Report No. 79-4, USAARL.

[5] Mell, W. E., and Lawson, J. R., 2000, "A Heat Transfer Model for Firefighters' Protective Clothing," Fire Technology, 36(1), pp. 39-68.

[6] Barker, R. L., Guerth-Schacher, C., Grimes, R. V., and Hamouda, H., 2006, "Effects of Moisture on the Thermal Protective Performance of Firefighter Protective Clothing in Low-Level Radiant Heat Exposures," Textile Research Journal, 76(1), pp. 27-31.

[7] Hirschler, M. M., 1997, "Analysis of Thermal Performance of Two Fabrics Intended for Use as Protective Clothing," Fire and Materials, 21(3), pp. 115-121.

[8] Song, G., 2007, "Clothing Air Gap Layers and Thermal Protective Performance in Single Layer Garment," Journal of Industrial Textiles, 36(3), pp. 193-205.

[9] Kim, I. Y., Lee, C., Li, P., Corner, B. D., and Paquette, S., 2002, "Investigation of Air Gaps Entrapped in Protective Clothing Systems," Fire and Materials, 26(3), pp. 121-126.

[10] Liter, S. G., Burgess, D. R., Kaviany, M., Wang, J. T., and Kang, J., 1998, "Transient Heating of Air Bag Fabrics: Experiment and Modeling,"SAE-980865.

[11] Liter, S. G., Park, C.-W., Kaviany, M., Wang, J. T., Kang, J., and Lee, Y. G., 1999, "An Experiment-Based Model of Fabric Heat Transfer and Its Inclusion in Air Bag Deployment Simulations," SAE-1999-01-0437.

[12] Liter, S. G., Kaviany, M., Wang, J. T., 1997, "Permeability and Transient Thermal Response of Airbag Fabrics," SAE-971063.

[13] ISO 17492, 2003, "Clothing for Protection against Heat and Flame – Determination of Heat Transmission on Exposure to Both Flame and Radiant Heat."

[14] ASTM D, 4108-82, "Standard Test Method for Thermal Protective Performance of Materials for Clothing by Open-Flame Method."

[15] ASTM F, 1939-99a, "Standard Test Method for Radiant Protective Performance of Flame Resistant Clothing Materials."

[16] ASTM E1461-7, "Standard Test Method for Thermal Diffusivity by the Laser Flash Method."

[17] ASTM E1269, "Standard Test Method for Determining Specific Heat Capacity by Differential Scanning Calorimetry."

[18] Martin, H., 1977, "Heat and Mass Transfer between Impinging Gas Jets and Solid Surfaces," Academic Press, Inc., New York.

[19] Whitaker, S., 1983, Fundamental Principles of Heat Transfer, Krieger Publishing Company.